Available online at www.sciencedirect.com
ScienceDirect
Journal of the European Ceramic Society 28 (2008) 2529–2538
www.elsevier.com/locate/jeurceramsoc

Microwave sintering of plasma-sprayed yttria stabilized zirconia electrolyte coating

Chao Zhang [a,b,*], Ga Zhang [a], Susanne Leparoux [c], Hanlin Liao [a], Cheng-Xin Li [b], Chang-Jiu Li [b], Christain Coddet [a]

[a] *LERMPS, Université de Technologie de Belfort-Montbéliard, 90010 Belfort, France*
[b] *State Key Laboratory for Mechanical Behavior of Materials, Xi'an Jiaotong University, Xi'an 710049, Shaanxi, China*
[c] *Swiss Federal Laboratories for Materials Testing and Research, Feuerwerkerstrasse 39, CH-3602 Thun, Switzerland*

Received 12 December 2007; received in revised form 25 March 2008; accepted 28 March 2008
Available online 19 May 2008

Abstract

In this work, microwave (MW) was used to sinter atmospheric plasma-sprayed 8 mol% yttria stabilized zirconia (YSZ) electrolytes coatings. Three types of coatings were studied: pure YSZ coating, 5 wt% $BaTiO_3$ filled YSZ coating and 10 wt% $BaTiO_3$ filled YSZ coating. Microstructures and ionic conductivities of as-sprayed and MW-sintered coatings were characterized. The results indicated that that the pure YSZ coating can hardly be sintered by the MW sintering and it can only be heated up to 900 °C. For two composite coatings, $BaTiO_3$ particles distributed in the composite coating act as a good MW susceptor and thereby, a good heat source for sintering YSZ matrix. After a MW sintering at 1450 °C for about 30 min, an obvious structural modification was noticed: the lamellar and columnar crystal features of as-sprayed plasma-sprayed YSZ coatings were modified to equiax crystal in the sintered coatings. Ionic conductivity of sintered 5 wt% $BaTiO_3$ filled YSZ composite coatings were elevated to about twice of as-sprayed coating. A further increase of $BaTiO_3$ content to 10 wt% in the composite coating enhanced the sintering efficiency, however, the ionic conductivity of composite coatings was decreased.

Keywords: Microwave processing; Sintering; Ionic conductivity; ZrO_2; Plasma spraying

1. Introduction

Recent developments in solid oxide fuel cells (SOFCs) show that the biggest challenge for its industrial application is to reduce manufacturing cost.[1] Therefore, the low cost manufacturing processes for SOFCs components are expected. At present, in most advanced SOFCs, 8 mol% yttria stabilized zirconia (YSZ) is widely used as electrolyte material due to its high performances in terms of oxygen ionic conductivity, thermal and chemical stability. Many technical routes, e.g. reactive sputter deposition, sol–gel, chemical vapor deposition (CVD), slurry coating and vacuum slip casting, were used to prepare YSZ electrolyte coatings.[2–4]

Plasma spraying is a promising method due to its high deposition rate, low cost and high flexibility. Low pressure plasma spraying (LPPS) and atmospheric plasma spraying (APS) are employed to deposit YSZ electrolyte coatings.[5–15] It has been pointed out that, compared with APS YSZ coating, LPPS YSZ coating has a higher ionic conductivity and lower gas permeability.[8] However, the relatively low cost of APS makes this technique more competitive.

A plasma-sprayed YSZ coating is formed by a stream of molten droplets impacting on a substrate. Individual molten droplets spread to thin lamellas, the stacking of which constitutes the deposit. As a result, a plasma-sprayed YSZ deposit is generally of lamellar structure. Pores, vertical cracks and non-bonded interfaces were always presented in the obtained YSZ coating.[16] Due to the lamellar structure and limited bonding characteristic between lamellae, as-sprayed coating always exhibits decreased mechanical and electrical properties. Previous studies indicate that the ionic conductivity of APS and LPPS YSZ electrolyte coating are about one-fifth to one-fourth of the bulk YSZ electrolyte.[13,17] In order to improve the coating electrical performance, some post-treatment techniques were

* Corresponding author.
E-mail addresses: chao.zhang@utbm.fr, zhangchao_cqu@hotmail.com (C. Zhang).

0955-2219/$ – see front matter © 2008 Elsevier Ltd. All rights reserved.
doi:10.1016/j.jeurceramsoc.2008.03.040

Table 1
Thermal properties of $BaTiO_3$ and ZrO_2

	Specific heat (J/g)	Thermal conductivity (W/m K)	Dielectric loss factor (2.45 GHz)	
	1000 °C	1000 °C	25 °C	1000 °C
$BaTiO_3$	0.59	2.2–3.2	180	>180
ZrO_2	0.64	2.2	0.0034	0.053

developed by means of conventional heat sintering,[18] chemical solution densification technique[13,19] and spark plasma sintering technique.[7,12]

Microwave (MW) sintering is a relatively new technique employed for sintering of ceramics. The advantage of MW sintering is volume heating and thereby, a uniform and rapid sintering is possible.[20] Additionally, compared with conventional sintering process in which heating begins from the material surface, MW sintering lowers thermomechanical stresses in materials due to more uniform heat distribution.[21] For a given material, the power absorbed per unit volume could be calculated as follow[22]:

$$P = 2\pi f \xi_0 \xi'' |E|^2 = 2\pi f \xi_0 \xi'_r \tan\delta |E|^2 \quad (1)$$

where E is the magnitude of the internal electrical field, ξ'' is the relative effective dielectric factor, ξ_0 is the permittivity of free space, f is the microwave frequency, ξ'_r is the relative dielectric constant, and $\tan\delta$ is the energy loss required to store a given quantity of energy. Product of $\xi_0\xi''$ (or $\xi_0\xi'_r \tan\delta$) is called dielectric loss factor. The dielectric loss factor determines the material coupling property, according to which materials can be classified into: transparent (low dielectric loss materials) – MW pass through with little, if any, attenuation; opaque (conductors) – MW are reflected and do not penetrate; and, absorbing (high dielectric loss materials) – absorb MW energy to a certain degree based on the value of dielectric loss factor.[21]

In general term, most ceramics have a low dielectric loss factor or are transparent to MW radiation. When a low dielectric loss factor material is subject to MW radiation, it may be heated up slowly and this can lead to a plasma formation in the cavity.[20] One solution for this problem is to use a susceptor installed together with the low dielectric loss factor material in the MW cavity.[20,23,24] Correspondingly, the heating mechanism is a combination of microwave heating and conventional heating by the filled susceptor. $BaTiO_3$ is an ideal candidate material for MW susceptor because of its high loss factors. The thermal properties and dielectric loss factor of $BaTiO_3$ and ZrO_2 are shown in Table 1.[20] It is clearly seen that $BaTiO_3$ is a good MW suspector candidate.

The investigations on MW sintering ceramic were very active in recent years, however, most of the previous efforts contributed to the sintering of bulk materials.[25–27] It could be pertinent to indicate that microwave sintering of plasma-sprayed YSZ electrolyte coatings was not reported before. In this paper, the feasibility of MW sintering on APS YSZ electrolyte coating was studied. With considering the low dielectric factor of YSZ, $BaTiO_3$ powders were incorporated into the YSZ powders to deposit composite coatings. $BaTiO_3$ is chosen as a MW suspector material due to its high dielectric loss factor and its excellent decomposition resistance as well. The latter characteristic is very important for plasma spraying process in which the feed-stock materials are subjected to a high temperature plasma flow. The as-sprayed YSZ and $BaTiO_3$–YSZ composite coatings were sintered using a MW furnace respectively. The influence of $BaTiO_3$ and its content on the sintering efficiency, coating structure and ionic conductivity were investigated.

2. Experimental

A commercially available 8 mol% YSZ powders (Marion technologies, France) was used as feedstock material. Fig. 1(a) illustrates the morphologies of the YSZ powders. Powder size

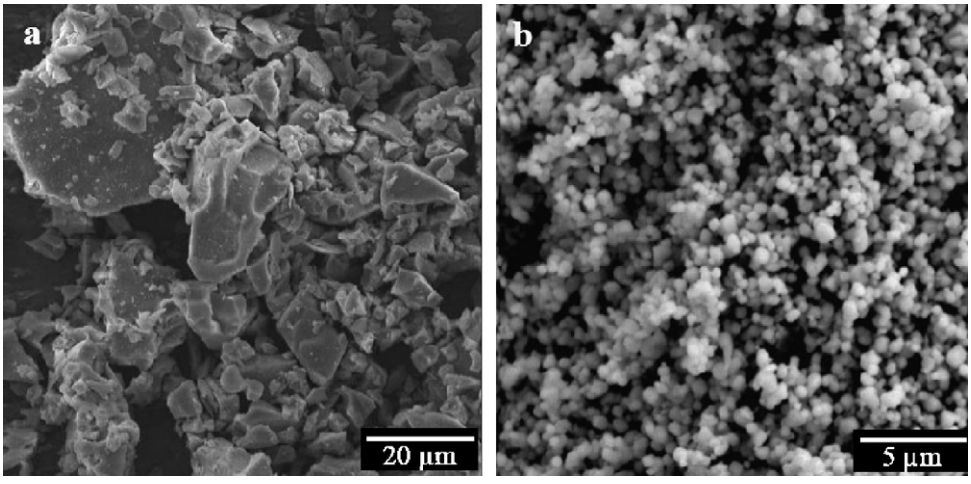

Fig. 1. SEM powder morphologies of: (a) YSZ and (b) $BaTiO_3$.

Table 2
APS parameters used for deposition of coatings

Current (A)	Power (kW)	Ar (SLPM)	H_2 (SLPM)	Carrier gas (Ar, SLPM)	Spray distance (mm)	Gun traverse speed (mm/s)
600	39.5	35	12	3.5	100	400

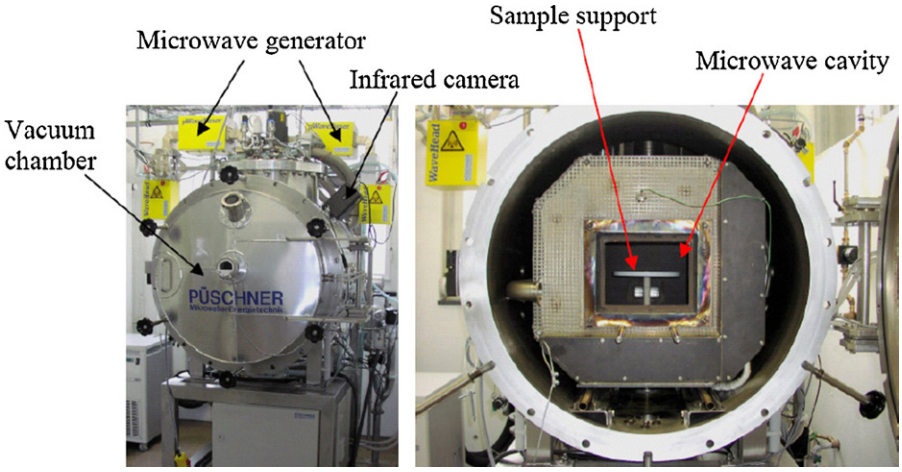

Fig. 2. Outline and inner structures of the microwave sintering system.

distribution was measured with a laser particle size analyzer (Mastersizer 2000, Malvern Instruments, UK). It exhibited a distribution with D10 of 4.88 μm, D50 of 25.60 μm and D90 of 58.71 μm.

$BaTiO_3$ powders (Inframat, USA) have an average diameter of about 0.7 μm. The morphology of this powder was shown in Fig. 1(b). Generally, only the powders with a diameter in the distribution of 5–100 μm can be used as feedstock for plasma spraying process. In order to increase the flowability of the fine powders, the small $BaTiO_3$ powders were agglomerated with 5 wt% PVA solution and were finally meshed to get a diameter range under 50 μm. Then, the powders were dried in a furnace at 200 °C for 2 h. The obtained agglomerated $BaTiO_3$ powders were incorporated into the YSZ powders with 5 and 10 wt% contents, respectively. The mixed powders were mechanically blended for 20 min to get a homogenous mixture.

Three types of coatings, pure YSZ, 5 wt% $BaTiO_3$–YSZ and 10 wt% $BaTiO_3$–YSZ, were deposited using an APS system (A-2000 with F4MB torch, Sulzer Metco AG, Switzerland). Powders were fed into plasma stream by 10-Twin systems (Plasma-Technik AG, Switzerland) during spraying. Spraying parameters are shown in Table 2. The coatings were deposited on aluminum plates of dimension 4 cm × 6 cm × 0.3 cm. Prior to spraying, the substrates were grit-blasted with alumina grits at a pressure of about 0.2 MPa. A robot (ABB, Sweden) was employed to move the torch in order to achieve a uniform and reproducible deposition. Thickness of as-sprayed coatings was controlled at about 800 μm. After deposition, the specimen was cut into squares of 1.5 cm × 1.5 cm with cutting machine (Accoton-5, Struers, USA). Then, the substrates of specimens were dissolved using a sodium hydroxide solution to obtain freestanding specimens for MW sintering.

The square freestanding coatings were positioned in a microwave sintering system (MW720, Püschner, Germany). The outline and inner structures of the microwave power system are shown in Fig. 2. In this work, sintering process was performed under an ambient pressure in air. Three 2.45 GHz microwave generators were adopted simultaneously to get a homogenous microwave field in the cavity. Power of three generators was 3000, 3000 and 1200 W, respectively. Coating surface temperature was measured by an infrared camera and was recorded dynamically with a computer.

Coating microstructures were examined before and after MW sintering by scanning electron microscopy (SEM, JSM-6360LV, JEOL, Japan). An energy dispersion spectroscopy (EDS) analysis was performed on coating cross-sections. The

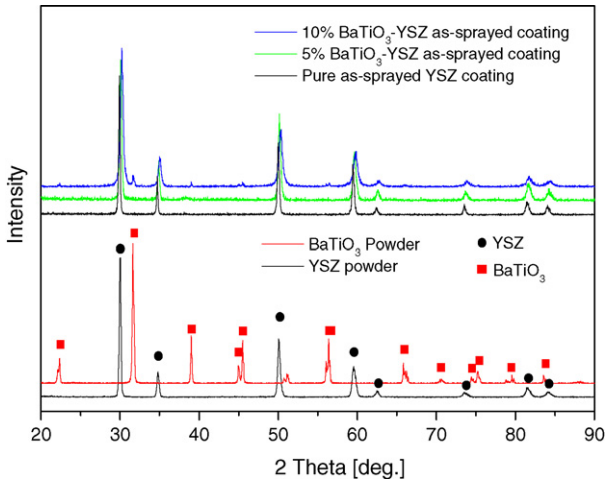

Fig. 3. XRD patterns of pure YSZ, 5 wt% $BaTiO_3$–YSZ, 10 wt% $BaTiO_3$–YSZ as-sprayed coatings with YSZ and $BaTiO_3$ powders.

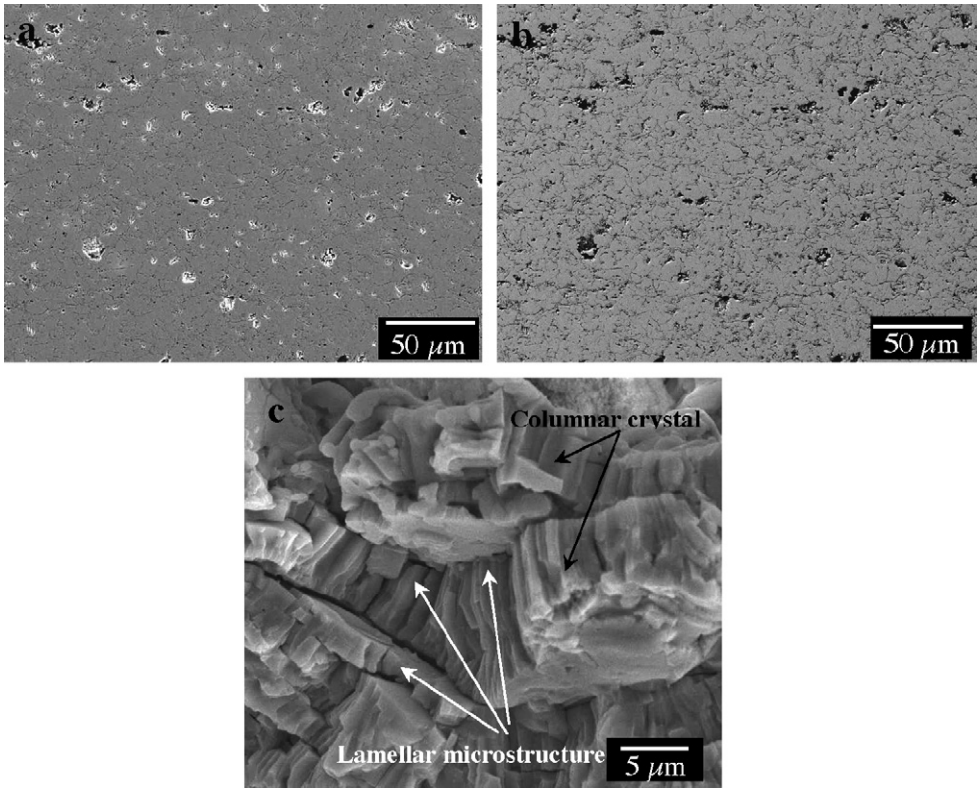

Fig. 4. SEM polished cross-section microstructure with SEI mode (a) and BEI mode (b), fractal cross-section microstructure (c) of pure YSZ as-sprayed coating.

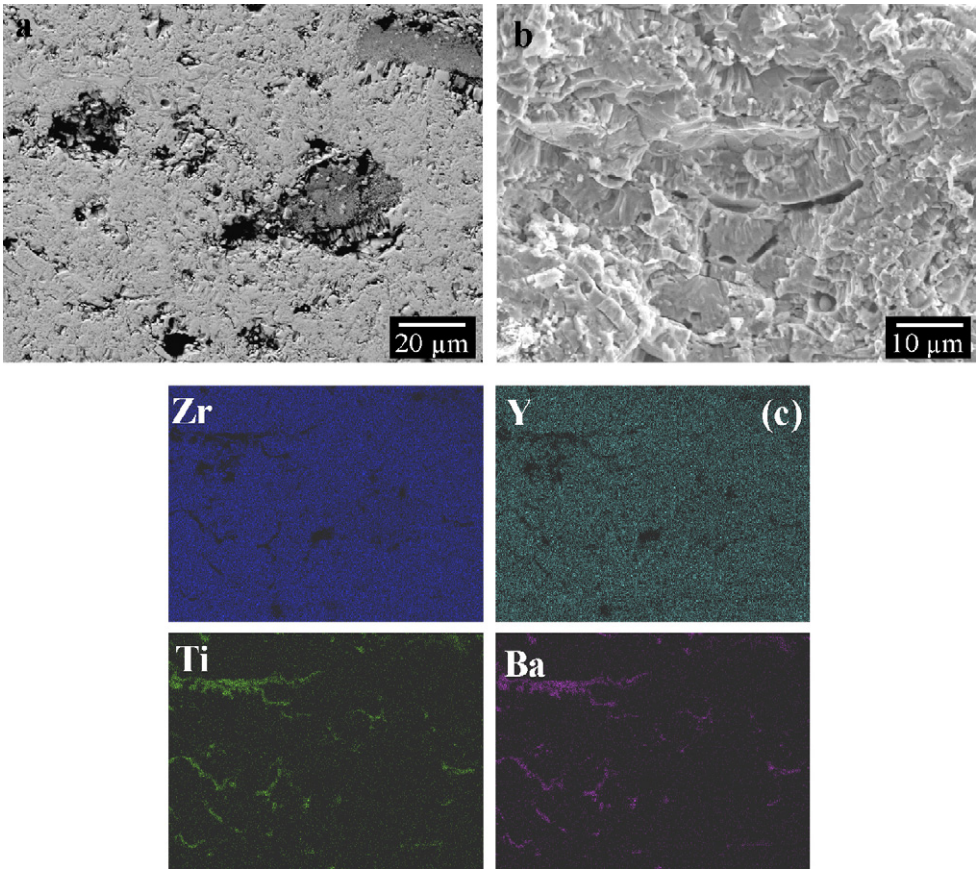

Fig. 5. SEM polished cross-section microstructure (a), SEM fractal cross-section microstructure (b), polished surface EDS chemical mapping analysis (c) and EDS chemical point analysis (d–f) of 5 wt% $BaTiO_3$–YSZ as-sprayed coating.

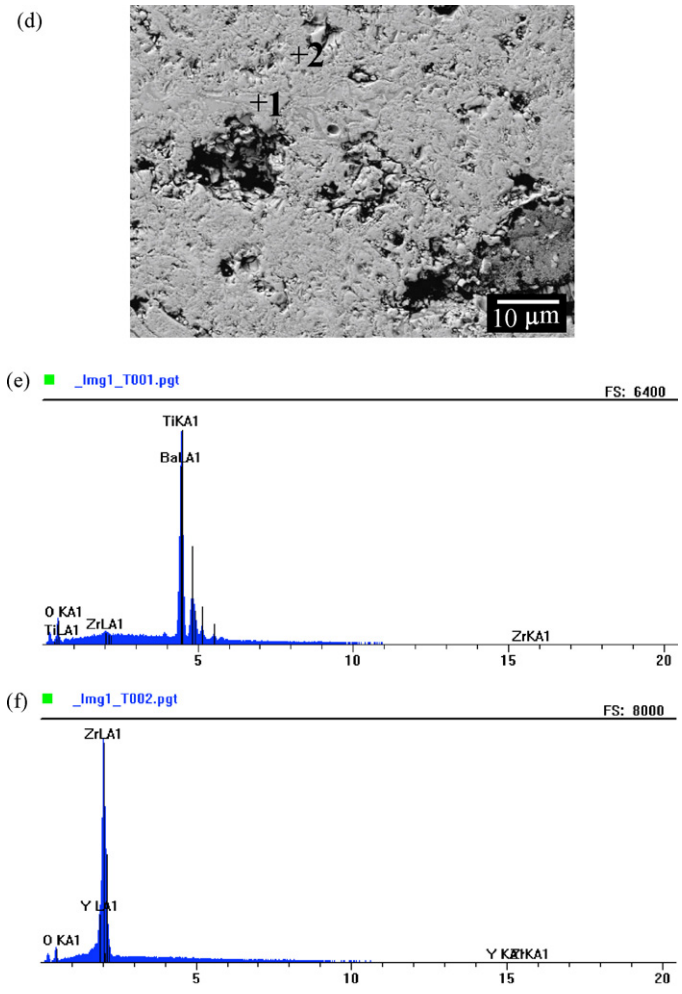

Fig. 5. (*Continued*).

phase constitutions of both powder coatings were characterized by X-ray diffraction analysis (XRD-6000, Shimadzu, Japan) using a Cu Kα radiation. A 2θ scanning rate of $5^\circ\,\mathrm{min}^{-1}$ was used during test.

Ionic conductivity of coatings was measured using a potentiostat/galvanostat based on a three-electrode assembly approach. To ensure the measuring area of the circular planar sample, platinum glue was pasted on both sides of the sample with a specific effective area of $1\,\mathrm{cm}^2$. The pasted sample was dried at 100 °C for 30 min and then heated to 900 °C with a heating rate of $5\,^\circ\mathrm{C\,min}^{-1}$ and kept at 900 °C for 30 min. According to the linear relation between current and potential difference, the resistivity and subsequently conductivity was determined.[13] More details on ionic conductivity measurement are available elsewhere.[7,8]

3. Results and discussion

3.1. Microstructure of as-sprayed plasma-sprayed YSZ coatings

Fig. 3 shows the XRD patterns of the as-sprayed coatings and the starting powders. Being consistent with the starting powders, YSZ coating consists of well-crystallized single cubic zirconia phase. For 5 wt% $BaTiO_3$–YSZ coating, no obvious $BaTiO_3$ peak was found. This was ascribed to the low content of $BaTiO_3$, since XRD analyzer was difficult to determine a low content phase (less than 5%) in composite materials. In contrast, $BaTiO_3$ peaks were clearly shown in the XRD patter of 10 wt% $BaTiO_3$–YSZ coating. Clearly, all the peaks in 10 wt% $BaTiO_3$–YSZ coating correspond to those in the $BaTiO_3$ and YSZ powders. This indicates that no phase transformation occurs in the plasma spraying process.

Fig. 4(a) shows polished cross-sectional microstructure of as-sprayed YSZ coating. It exhibits a relatively dense structure. For increasing contrast between YSZ and coating defaults, detection with backscattered election image (BEI) mode was used as shown in Fig. 4(b). Fig. 4(c) shows the fractal cross-sectional microstructure of the as-sprayed YSZ coating. It can be found that the YSZ coating shows a typical plasma-sprayed ceramic coating, which has a lamellar microstructure (as labelled in Fig. 4(c)) and presents columnar crystal microstructure in a single lamella. These structural features are closely related to the APS spraying features, in which a deposit is formed by a stream of molten droplets impacting on the substrate. The lamellar structure of the coating with limited lamellar interface

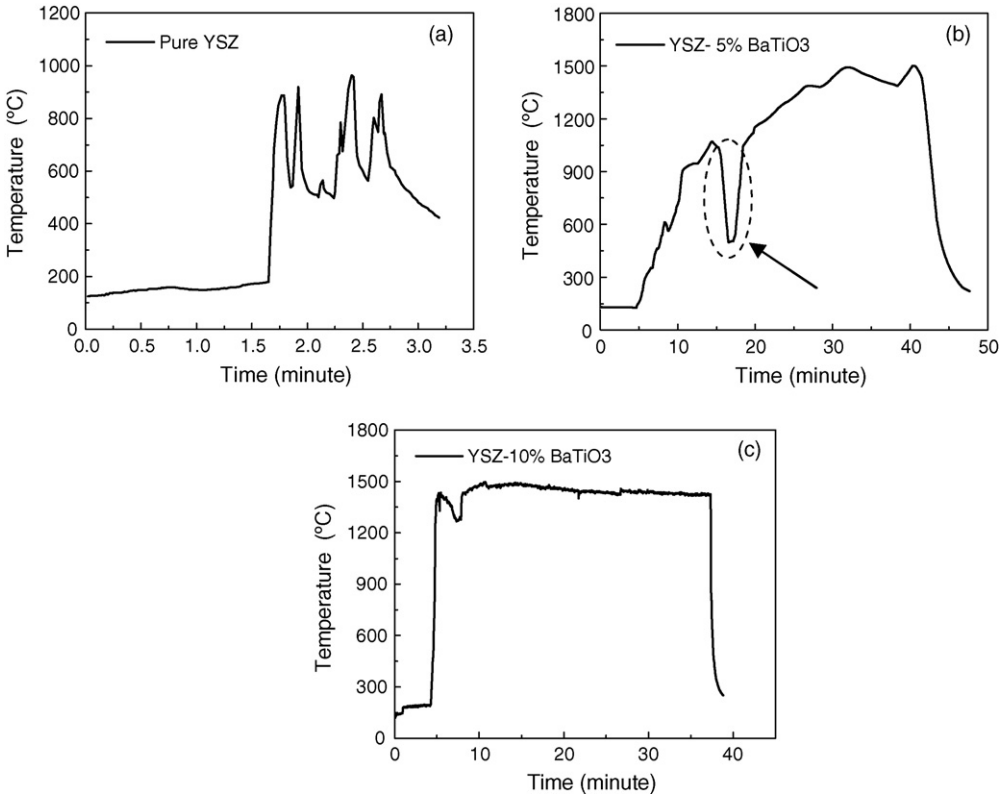

Fig. 6. Temperature recording of pure YSZ (a), 5 wt% $BaTiO_3$–YSZ (b), 10 wt% $BaTiO_3$–YSZ (c) coating surfaces during MW heating.

bonding and vertical cracks leads to an anisotropy of coating properties and also a reduction of ionic conductivity.[13,17]

Fig. 5(a) and (b) shows polished and fractal cross-sectional structures of 5 wt% $BaTiO_3$–YSZ as-sprayed coating. Being alike to the pure YSZ coating, the composite coating also has a lamellar microstructure. Fig. 5(c) gives the distributions of the elements Zr, Y, Ti, Ba determined by the EDS chemical mapping analysis of the composite coating. The distribution of Ba shows

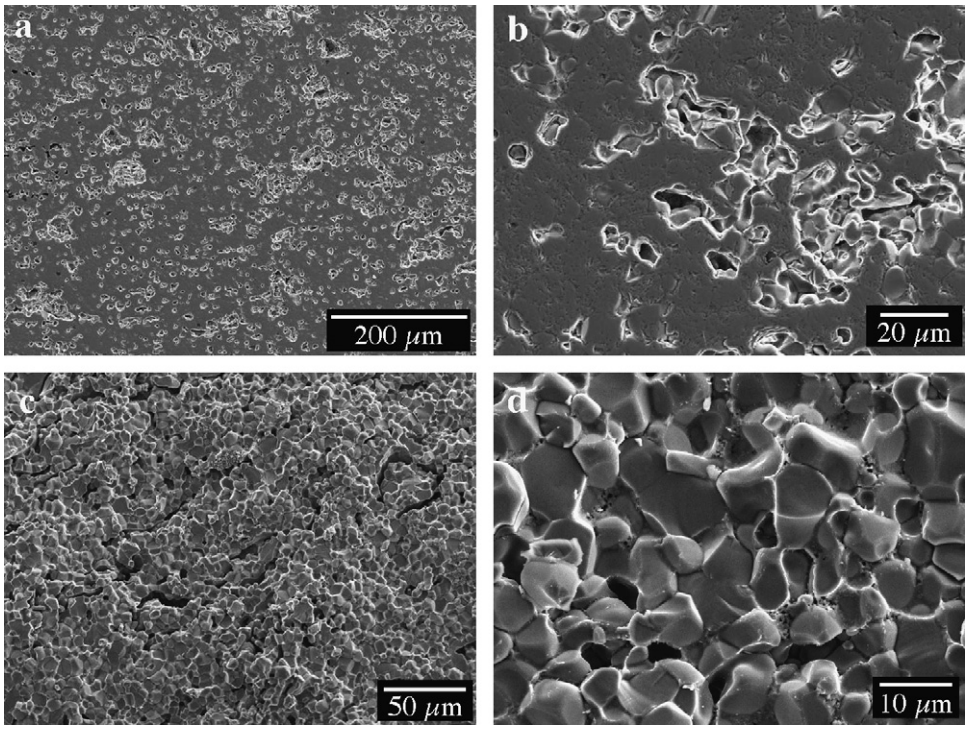

Fig. 7. SEM polished cross-section (a and b) and fractal cross-section (c and d) microstructure of 5 wt% $BaTiO_3$–YSZ MW sintered coating.

that the $BaTiO_3$ was well melted and flatted during the spraying process. Further to observe the microstructure of the composite coating in high resolution and chemical point mapping analysis as shown in Fig. 5(d)–(f), it could be verified that $BaTiO_3$ powders were well molten and flatted in the as-sprayed coating, which was confirmed by EDS chemical point analysis.

3.2. MW sintering

The three types of freestanding coatings were sintered in the microwave sintering system. Fig. 6(a) shows heating curve of pure YSZ coating during MW sintering. The pure YSZ coating can only be heated to less than 900 °C. The limited heating efficiency was attributed to the low dielectric loss factor of pure YSZ material. Regardless the significant increase of the dielectric loss factor when increasing temperature, even at a temperature of 1000 °C, the factor of YSZ is still very low (0.053[20]). During MW heating process, much MW energy was absorbed by the atmosphere instead of the YSZ sample. This results in a plasmas formation in the cavity. Additionally, a heat transfer occurs between the sample and the environment. When the heat transfer energy equals to that of sample absorbed from MW radiation, the coating temperature could not be further elevated.

Compared with pure YSZ coating, 5 wt% $BaTiO_3$–YSZ and 10 wt% $BaTiO_3$–YSZ coatings can be heated to 1450 °C rapidly. As seen from the comparison of Fig. 6(b) and (c), an increase in $BaTiO_3$ content leads to a higher heating efficiency of the coating. Moreover, as marked in the Fig. 6(b), a fluctuation was observed on the heating curve. This may be caused by plasma formation during the early stage of microwave sintering of 5 wt% $BaTiO_3$–YSZ coating. In high temperature region, there is no fluctuation found on the heating curve. As aforementioned, in the high temperature range, the composite coating has a higher dielectric loss factor and this may be the reason why no plasma formation in late stage.

For the composite coatings, the sintering of YSZ matrix can be considered as a hybrid heating: by traditional heat transfer and by MW radiation. During MW sintering process, $BaTiO_3$ phase were heated preferentially and presented a higher temperature than YSZ matrix. As a result, $BaTiO_3$ could be regarded as traditional thermal sources for the YSZ matrix and therefore heat transfer from the $BaTiO_3$ particles to the matrix occurs. If the heat exchange between the sample and the environment was not considered, the following equation can be obtained:

$$\frac{dT}{dt} = \frac{PV - Q_e}{\rho VC} = \frac{2\pi f \xi_0 \xi'' |E|^2 V - Q_e}{\rho VC} \quad (2)$$

where Q_e is the heat transfer from the $BaTiO_3$ to YSZ materials by means of thermal conduction, heat radiation and convection; T is the temperature of $BaTiO_3$ and t is the time; ρ and C represent respectively the massive density and the heat capacity of $BaTiO_3$; V is the volume of $BaTiO_3$ phase.

3.3. Microstructure of MW-sintered coatings

Fig. 7(a) and (b) shows polished cross-sectional microstructure of MW-sintered 5 wt% $BaTiO_3$–YSZ composite coatings in a low and high resolution. The sintered coating exhibits a distinct structure from that of the as-sprayed one. Only independent pores were present in the sintered coating. Fig. 7(c) and (d) shows fractal microstructure of the sintered coating. It was clearly observed that the sintered coating shows equiax crystal structure, which was very different from the lamellar structure of the as-sprayed coating. Pores were apparent between the equiax crystals. After MW sintering, intrinsic features of as-sprayed YSZ coating, such as non-bonded interface and vertical cracks, have disappeared. The structural modification has a significant effect on coating ionic conductivity. This will be discussed in the next section.

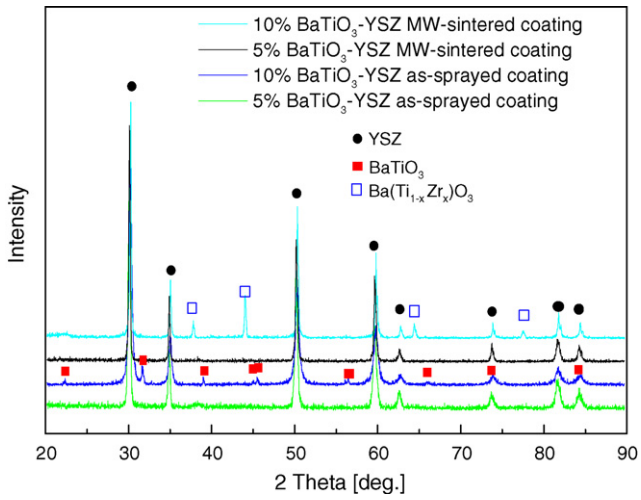

Fig. 8. XRD patterns of 5 wt% $BaTiO_3$–YSZ and 10 wt% $BaTiO_3$–YSZ MW-sintered coatings with their as-sprayed coatings.

Fig. 8 shows XRD patterns of MW-sintered 5 wt% $BaTiO_3$–YSZ and 10 wt% $BaTiO_3$–YSZ composite coatings compared with the as-sprayed coatings. Only YSZ phase was detected in the XRD pattern in both as-sprayed and MW-sintered 5 wt% $BaTiO_3$–YSZ coatings due to the low $BaTiO_3$ content. With respect to the 10 wt% $BaTiO_3$–YSZ coatings, $BaTiO_3$ and YSZ phases were clearly noticed in the XRD patterns of the as-sprayed and sintered coatings. However, it should be noted that a new phase $Ba(Ti_{1-x}Zr_x)O_3$ is apparent in the MW sintered coating. The substitution of Ti^{4+} in $BaTiO_3$ with Zr^{4+} in YSZ is completed during sintering process, which was confirmed by XRD and Raman spectroscopy in other study.[28]

An EDS chemical mapping analysis of the MW-sintered 10 wt% $BaTiO_3$–YSZ coating was conducted as shown in Fig. 9. Interestingly, compared with Fig. 5(c), an aliquation of $BaTiO_3$ ($Ba(Ti_{1-x}Zr_x)O_3$) phase occurs and $BaTiO_3$ ($Ba(Ti_{1-x}Zr_x)O_3$) phase tends to assemble in the interface of equaix crystals. This can be attributed to the distinct difference of the melting points of the two materials (1640 and 2700 °C for $BaTiO_3$ and YSZ, respectively).

3.4. Ionic conductivity

Fig. 10 shows the ionic conductivities of the three as-sprayed coatings measured from 600 to 1000 °C. Ionic conductivity of pure YSZ as-sprayed sample was 0.035 S/cm at 1000 °C. This is

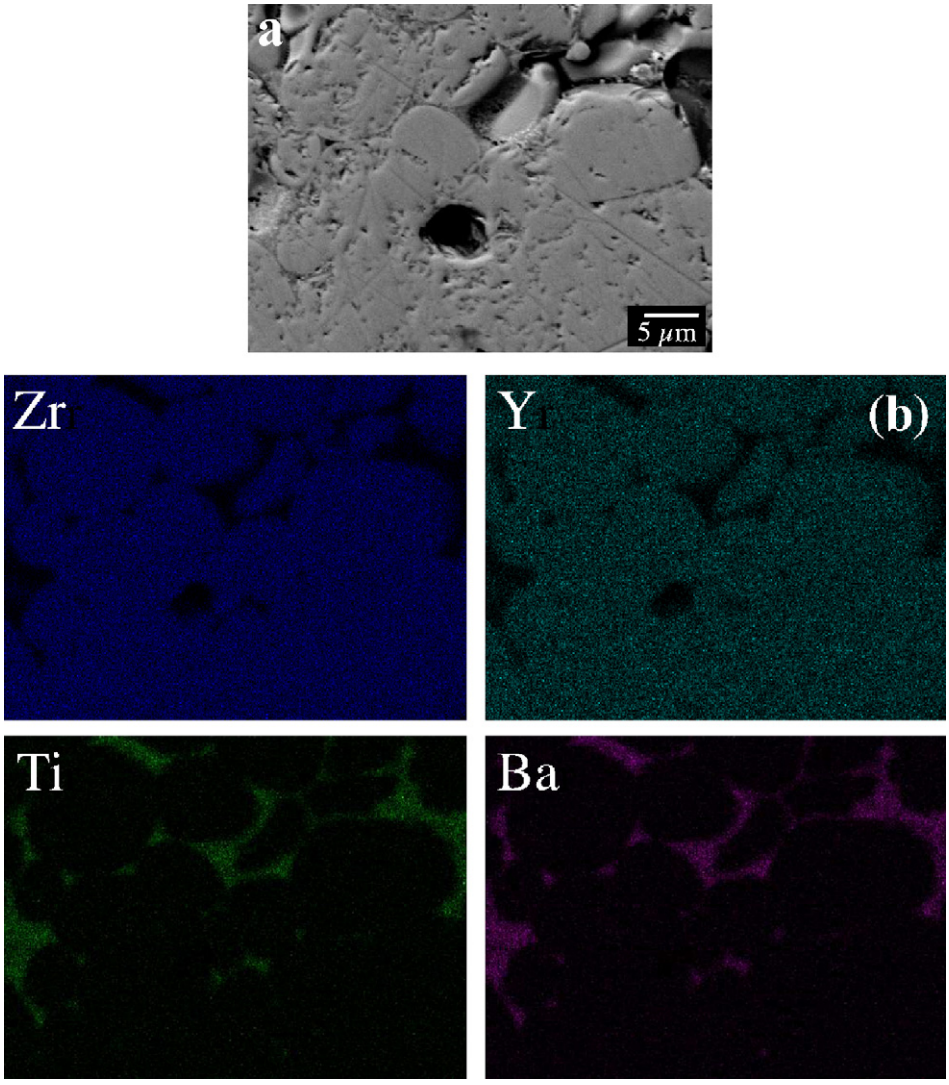

Fig. 9. Polished cross-section surface EDS chemical mapping analysis (a and b) of 5 wt% $BaTiO_3$–YSZ MW-sintered coating.

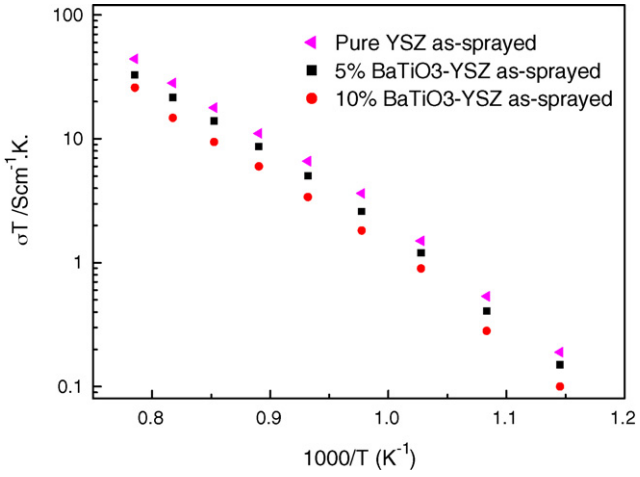

Fig. 10. Arrhenius relation of σT and $1000\,T^{-1}$ for the YSZ, 5 wt% $BaTiO_3$–YSZ and 10 wt% $BaTiO_3$–YSZ as-sprayed coatings.

consistent with the results in our previous study.[13,17] $BaTiO_3$, as an insulator in the composite coating, interrupts the oxygen ionic conduction in YSZ matrix and consequently decrease the coating ionic conductivity. It can be found that ionic conductivity of the as-sprayed 5 wt% $BaTiO_3$–YSZ and 10 wt% $BaTiO_3$–YSZ samples are 0.026 and 0.020 S/cm at 1000 °C, respectively.

Fig. 11 shows the ionic conductivity of MW-sintered 5 wt% $BaTiO_3$–YSZ and 10 wt% $BaTiO_3$–YSZ coatings compared to those of the as-sprayed pure YSZ coatings. After MW sintering, the ionic conductivities of the 5 wt% $BaTiO_3$–YSZ and 10 wt% $BaTiO_3$–YSZ coatings are enhanced to 0.054 and 0.035 S/cm at 1000 °C, respectively. These values are about twice of the as-sprayed coatings. Compared with the pure YSZ coating, the MW-sintered 5 wt% $BaTiO_3$–YSZ coating exhibits a higher ionic conductivity by about 60%. The improvement of ionic conductivity is related to the structural modification after MW heating. After MW sintering, the lamellar microstructure was modified to equiax crystal. The bonding ratio between the lamellae was significantly improved and thus the ionic conductivity was increased. However, for the MW-sintered 10 wt% $BaTiO_3$–YSZ coating, the ionic conductivity is only comparable to the as-sprayed pure YSZ coating. As aforementioned, too

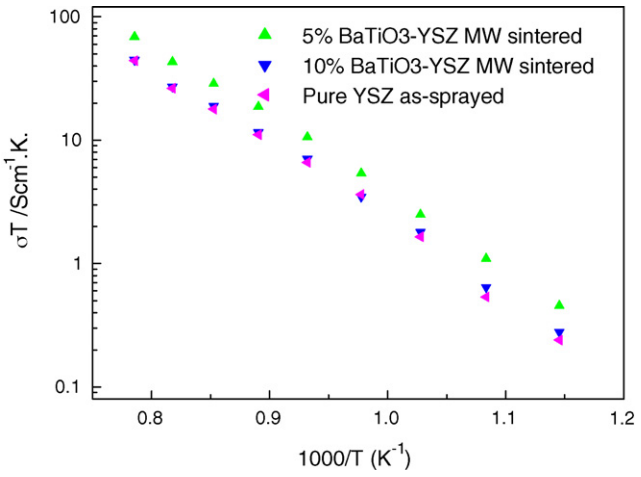

Fig. 11. Arrhenius relation of σT and $1000\,T^{-1}$ for the YSZ as-sprayed, 5 wt% $BaTiO_3$–YSZ and 10 wt% $BaTiO_3$–YSZ MW-sintered coatings.

much $BaTiO_3$ content could interrupt ionic conduction in YSZ matrix and restrict the improvement of ionic conductivity of composite coating.

4. Conclusions

In this study, the feasibility of MW sintering on APS YSZ coatings, with $BaTiO_3$ as MW susceptor, was investigated. Follow conclusions can be drawn:

(1) Pure APS YSZ coating can only be heated to less than 900 °C in the MW cavity due to its low dielectric loss factor, whereas the $BaTiO_3$–YSZ composite coating could be easily heated to 1450 °C.
(2) For the $BaTiO_3$–YSZ composite coating, the $BaTiO_3$ particles were regarded as distributed heat sources in YSZ matrix. The lamellar structure of the as-sprayed $BaTiO_3$–YSZ composite coatings is modified to equiax crystal in MW-sintered coatings. $BaTiO_3$ transformed to $Ba(Ti_{1-x}Zr_x)O_3$ during MW sintering process and assembles to the interface after MW sintering.
(3) Ionic conductivity of MW-sintered composite coatings was about one time higher than that of as-sprayed coatings. Compared with ionic conductivity of the pure YSZ coating, the MW-sintered 5 wt% $BaTiO_3$–YSZ coating presented a 60% higher conductivity.

Acknowledgements

This work was financially supported by the French Ministry of Research (Program APURoute, No.: 04F364). One of the authors (Chao Zhang) wish to thank the co-tutors scholarship of French Government (Bourse du Gouvernement Français pour les cotutelles de thèse). Authors are grateful to Sebastian Paris of Swiss Federal Laboratories for Materials Testing and Research for his assistance of microwave sintering.

References

1. Steele, B. C. H., Materials science and engineering: the enabling technology for the commercialisation of fuel cell systems. *J. Mater. Sci.*, 2001, **36**(5), 1053–1068.
2. Will, J., Mitterdorfer, A., Kleinlogel, C., Peredis, D. and Gauckler, L. J., Fabrication of thin electrolytes for second-generation solid oxide fuel cells. *Solid State Ionics*, 2000, **131**(1–2), 79–96.
3. Basu, R. N., Blass, G., Buchkremer, H. P., Stöver, D., Tietz, F., Wessel, E. *et al.*, *J. Eur. Ceram. Soc.*, 2005, **25**(4), 463–471.
4. Xu, X., Xia, C., Huang, S. and Peng, D., YSZ thin films deposited by spin-coating for IT-SOFCs. *Ceram. Internat.*, 2005, **31**(8), 1061–1064.
5. Lang, M., Franco, T., Schiller, G. and Wagner, N., Electrochemical characterization of vacuum plasma sprayed thin-film solid oxide fuel cells (SOFC) for reduced operating temperatures. *J. Appl. Electrochem.*, 2002, **32**(8), 871–874.
6. Li, C. J., Li, C. X., Xing, Y. Z., Gao, M. and Yang, G.-J., Influence of YSZ electrolyte thickness on the characteristics of plasma-sprayed cermet supported tubular SOFC. *Solid State Ionics*, 2006, **177**(19–25), 2065–2069.
7. Khor, K. A., Chen, X. J., Chan, S. H. and Yu, L. G., Microstructure-property modifications in plasma sprayed 20 wt.% yttria stabilized zirconia electrolyte by spark plasma sintering (SPS) technique. *Mater. Sci. Eng. A*, 2004, **366**(1), 120–126.
8. Zhang, C., Liao, H., Li, W. Y., Zhang, G., Coddet, C., Li, C.-J. *et al.*, Characterization of YSZ SOFC electrolyte deposited by atmospheric plasma spraying and low pressure plasma spraying. *J. Therm. Spray Technol.*, 2006, **15**(4), 598–603.
9. Fehringer, G., Janes, S., Wildersohn, M. and Clasen, R., Proton-conducting ceramics as electrode/electrolyte -materials for SOFCs: Preparation, mechanical and thermal-mechanical properties of thermal sprayed coatings, material combination and stacks. *J. Eur. Ceram. Soc.*, 2005, **24**(5), 705–715.
10. Notomi, A. and Histome, N., Application of plasma spraying to solid oxide fuel cell production. *Pure Appl. Chem.*, 1996, **68**, 1101–1106.
11. Tietz, F., Buchkremer, H. P. and Stöver, D., Components manufacturing for solid oxide fuel cells. *Solid State Ionics*, 2002, **152–153**, 373–381.
12. Khor, K. A., Yu, L.-G., Chan, S. H. and Chen, X. J., Densification of plasma sprayed YSZ electrolytes by spark plasma sintering (SPS). *J. Eur. Ceram. Soc.*, 2003, **23**(11), 1855–1863.
13. Li, C.-J., Ning, X.-J. and Li, C.-X., Effect of densification processes on the properties of plasma-sprayed YSZ electrolyte coatings for solid oxide fuel cells. *Surf. Coat. Technol.*, 2005, **190**(1), 60–64.
14. Tsukuda, H., Notomi, A. and Hisatome, N., Application of plasma spraying to tubular-type solid oxide fuel cells production. *J. Therm. Spray Technol.*, 2000, **9**(3), 364–368.
15. Singhal, S. C., Advances in solid oxide fuel cell technology. *Solid State Ionics*, 2000, **135**(1–4), 305–313.
16. Li, C.-J. and Ohmori, A., Relationships between the microstructure and properties of thermally sprayed deposits. *J. Therm. Spray Technol.*, 2002, **11**(3), 365–374.
17. Zhang, C., Li, C. J., Zhang, G., Ning, X. J., Li, C.-X., Liao, H. *et al.*, Ionic conductivity and its temperature dependence of atmospheric plasma-sprayed yttria stabilized zirconia electrolyte. *Mater. Sci. Eng. B*, 2007, **137**(1–3), 24–30.
18. Okumura, K., Aihara, Y., Ito, S. and Kawasaki, S., Development of thermal spraying-sintering technology for solid oxide fuel cells. *J. Therm. Spray Technol.*, 2000, **9**(3), 354–359.
19. Ning, X. J., Li, C. X., Li, C. J. and Yang, G. J., Modification of microstructure and electrical conductivity of plasma-sprayed YSZ deposit through post-densification process. *Mater. Sci. Eng. A*, 2006, **428**(1–2), 98–105.
20. Zhao, C., Vleugels, J., Groffils, G., Luypaert, P. J. and Van Der Biest, O., Hybrid sintering with a tubular susceptor in a cylindrical single-mode microwave furnace. *Acta Mater.*, 2000, **48**(14), 3795–3801.
21. Mizuno, M., Obata, S., Takayama, S., Ito, S., Kato, N., Hirai, T. *et al.*, Sintering of alumina by 2.45 GHz microwave heating. *J. Eur. Ceram. Soc.*, 2004, **24**(2), 387–391.
22. Sutton, W. H., Microwave processing of ceramic materials. *Am. Ceram. Soc. Bull.*, 1989, **68**(2), 376–386.

23. Zhang, G., Leparoux, S., Liao, H. and Coddet, C., Microwave sintering of poly-ether-ether-ketone (PEEK) based coatings deposited on metallic substrate. *Scripta Mater.*, 2006, **55**(7), 621–624.
24. Kesapragada, S. V., Bhaduri, S. B., Bhaduri, S. and Singh, P., Densification of LSGM electrolytes using activated microwave sintering. *J. Power Sources*, 2003, **124**(**2**), 499–504.
25. Huang, S. G., Li, L., Van der Biest, O. and Vleugels, J., Microwave sintering of CeO_2 and Y_2O_3 co-stabilised ZrO_2 from stabiliser-coated nanopowders. *J. Eur. Ceram. Soc.*, 2007, **27**(2-3), 689–693.
26. Binner, J., Annapoorani, K., Paul, A., Santacruz, I. and Vaidhyanathan, B., Dense nanostructured zirconia by two stage conventional/hybrid microwave sintering. *J. Eur. Ceram. Soc.*, 2008, **28**(5), 973–977.
27. Upadhyaya, D. D., Ghosh, A., Gurumurthy, K. R. and Prasad, R., Microwave sintering of cubic zirconia. *Ceram. Internat.*, 2001, **27**(4), 415–418.
28. Liu, X. Q. and Chen, X. M., Microstructures and mechanical properties of 8Y-FSZ ceramics with $BaTiO_3$ additive. *Ceram. Internat.*, 2004, **30**(8), 2269–2275.